Resonant superfluidity in an optical lattice

Titvinidze, I.; Snoek, M.; Hofstetter, W.

DOI
10.1088/1367-2630/12/6/065030
Publication date
2010
Document Version
Final published version
Published in
New Journal of Physics

Resonant superfluidity in an optical lattice

2010 New J. Phys. 12 065030

(http://iopscience.iop.org/1367-2630/12/6/065030)

New Journal of Physics
The open-access journal for physics

Resonant superfluidity in an optical lattice

I Titvinidze[1,3], M Snoek[2] and W Hofstetter[1]

[1] Institut für Theoretische Physik, Johann Wolfgang Goethe-Universität, 60438 Frankfurt am Main, Germany
[2] Institute for Theoretical Physics, Valckenierstraat 65, 1018 XE Amsterdam, The Netherlands
E-mail: irakli@itp.uni-frankfurt.de

New Journal of Physics **12** (2010) 065030 (20pp)
Received 8 December 2009
Published 28 June 2010
Online at http://www.njp.org/
doi:10.1088/1367-2630/12/6/065030

Abstract. We have studied a system of ultracold fermionic potassium (^{40}K) atoms in a three-dimensional (3D) optical lattice in the vicinity of an s-wave Feshbach resonance. Close to resonance, the system is described by a multi-band Bose–Fermi Hubbard Hamiltonian. We derive an effective lowest-band Hamiltonian in which the effect of higher bands is incorporated by a self-consistent mean-field approximation. The resulting model is solved by means of generalized dynamical mean-field theory. In addition to the BEC–BCS crossover, we find a phase transition to a fermionic Mott insulator at half-filling, induced by the repulsive fermionic background scattering length. We also calculate the critical temperature of the BEC/BCS state and find it to be minimal at resonance.

[3] Author to whom any correspondence should be addressed.

Contents

1. Introduction

The first experimental realizations of Bose–Einstein condensates (BEC) in dilute atomic gases of rubidium [1], lithium [2] and sodium [3] atoms initiated a new field of condensed-matter research, providing an ideal laboratory for comparing theoretical models and experimental results with high accuracy. In particular, the important consequences of Bose–Einstein condensation could be investigated, which up to 1995 had remained an elusive and inaccessible phenomenon in experiments.

Not long after the first realization of BEC, ultracold fermionic gases were studied experimentally as well. The first important results of quantum degeneracy in trapped Fermi gases were obtained in 1999 at JILA [4] and later on by other groups [5, 6]. A breakthrough experiment in this field was the investigation of fermionic superfluidity at the crossover between the BEC state and the Bardeen–Cooper–Schrieffer (BCS) state [7–11]. This was made possible by the use of Feshbach resonances, which have become an indispensable experimental tool for ultracold atom experiments. Feshbach resonances not only allow one to tune the interatomic interaction with high precision, but also make it possible to increase it to a level where the critical temperature becomes high enough for the investigation of attraction-induced superfluidity. In contrast, away from resonance the critical temperature is usually exponentially suppressed and experimentally inaccessible. The regime of strong, even diverging interactions, the so-called unitarity region, on the other hand, defines a new field of research where standard mean-field methods break down and the physics has to be described in a non-perturbative way. Moreover, this system allows for the experimental investigation of the BEC–BCS crossover: for negative scattering lengths the system is a BCS superfluid, whereas for positive scattering lengths, fermionic atoms with opposite spin pair up to form a bosonic molecular bound state. More recent experimental work has focused on the study of the effect of spin imbalance on the BCS state, i.e. the case when an unequal number of fermions occupies the two different spin states [12–15], as well as mixtures of fermions with unequal masses, such as ^{6}Li and ^{40}K [16, 17].

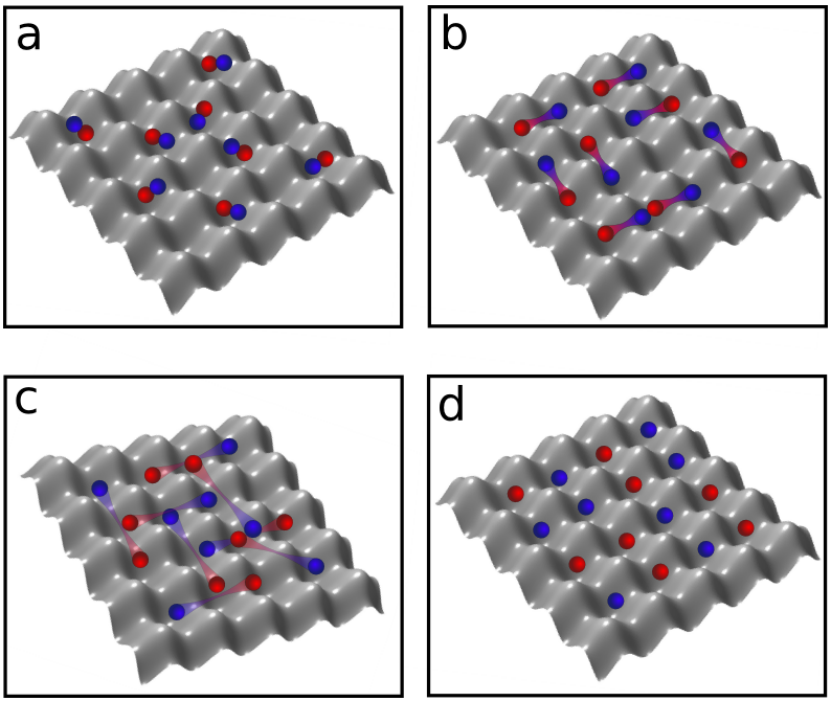

Figure 1. Schematic picture of the BEC–BCS crossover in an optical lattice. By tuning the interaction strength between the two fermionic spin states, one obtains a smooth crossover from a BEC regime of tightly bound bosonic molecules (a) to a BCS regime of large Cooper pairs (c). In between these two extremes, one encounters an intermediate crossover regime where the pair size is comparable with the interparticle spacing (b). For the total fermionic filling one, the system can undergo a phase transition to the Mott insulator phase (d).

Also, the effect of periodic potentials on trapped Fermi gases has been studied experimentally [18–21]. Recently, evidence for a fermionic Mott insulator was obtained in a system of repulsively interacting ^{40}K fermions in an optical lattice [22, 23]. Optical lattices and Feshbach resonances have been combined experimentally as well: the group at ETH Zürich reported the production of ^{40}K molecules in three-dimensional (3D) cubic optical lattices using s-wave Feshbach resonances in early 2006 [19], but no evidence of a superfluid state in the lattice was found until later that year, when superfluid ^{6}Li was loaded in an optical lattice at MIT where both a condensate and an insulating state were observed [20]. The results were interpreted in terms of a superfluid-to-Mott insulator transition, for which a detailed theoretical description is still lacking.

In this work, we study an ultracold mixture of fermionic atoms in two different hyperfine states in a 3D optical lattice close to a Feshbach resonance. This system has all the characteristics of the continuum BEC–BCS crossover described above: for magnetic field values below the resonance, fermions with different spins form bosonic molecules (see figure 1). By varying the magnetic field, the bosonic level is detuned relative to the fermionic one, which changes the ratio of the densities of fermions and molecular bosons as well as the effective interaction between the fermions. On top of this BEC–BCS crossover physics, which is familiar from the system without lattice, new features emerge when an optical lattice is applied. The

most prominent one is the occurrence of a fermionic Mott insulator for half-filled fermions deep in the BCS regime, which is stabilized by the repulsive fermionic background scattering length. As described below, we find a first-order transition between the BEC/BCS state and the Mott insulator. For a total filling of two fermions per site, the BCS state competes against a band insulating state [24–26].

The presence of an optical lattice allows one to utilize the powerful non-perturbative methods that are available for lattice systems. Here we apply generalized dynamical mean-field theory (GDMFT) [27, 28] to the system described above. However, GDMFT is a single-band approach, whereas Feshbach-resonant interactions in an optical lattice lead to a multi-band model [34–39]. We therefore first perform a mean-field decoupling of the higher bands, thereby deriving an effective single-band Hamiltonian that is self-consistently coupled to the higher bands.

The paper is organized as follows. In section 2, we introduce the microscopic model, and in section 3, we introduce the Generalized Dynamical Mean-Field approach we used to solve this model. In section 4, we present the result of our numerical calculations, and in section 5, we present the concluding remarks. In the appendix, we describe in detail how the self-energy for the resonantly interacting Bose–Fermi mixture studied here can be calculated in the dynamical mean-field framework.

2. Microscopic model

The study of ultracold fermions close to a Feshbach resonance is a challenging problem. Due to the fact that exactly on resonance the scattering length is infinite, the standard fermionic Hubbard Hamiltonian cannot be defined. To solve this problem, it is necessary to formulate a two-channel Hamiltonian by separating out the resonance state and treating it explicitly [40]. The nonresonant contributions give rise to a background scattering length. As the Feshbach resonance occurs due to a coupling with the bosonic molecular state, the additional degrees of freedom introduced in the two-channel theory are bosons [40].

An ultracold atomic gas of fermionic atoms and molecular bosons close to a Feshbach resonance in the presence of an optical lattice is thus well described by a Bose–Fermi Hubbard model [35, 41]. In our calculation, we assume the molecular bosons to be in the lowest band. For the fermions, on the other hand, we also have to take into account the higher bands, in order to properly incorporate the two-body physics associated with the Feshbach resonance [35, 36, 42]. Since the bandwidth is much smaller than the band gap, we approximate the higher bands to be flat and only take into account the full band structure for the lowest band. Moreover, we neglect the interaction between fermions in higher bands with each other and with the bosons. This is justified because the filling in the higher bands is very small, so that interaction effects are also small. The Hamiltonian thus has the following form:

$$\hat{\mathcal{H}} = \hat{\mathcal{H}}_{\mathrm{f}}^{0} + \hat{\mathcal{H}}_{\mathrm{b}} + \hat{\mathcal{H}}_{\mathrm{fb}}^{0} + \sum_{l=1}^{\infty} (\hat{\mathcal{H}}_{\mathrm{f}}^{l} + \hat{\mathcal{H}}_{\mathrm{fb}}^{l}), \tag{1}$$

$$\hat{\mathcal{H}}_{\mathrm{f}}^{0} = -t_{\mathrm{f}} \sum_{\langle ij \rangle} \hat{c}_{i\sigma,0}^{\dagger} \hat{c}_{j\sigma,0} + U_{\mathrm{f}} \sum_{i} \hat{n}_{i,\uparrow,0}^{\mathrm{f}} \hat{n}_{i,\downarrow,0}^{\mathrm{f}} - \left(\mu - \frac{3\hbar\omega}{2}\right) \sum_{i} \hat{n}_{i,0}^{\mathrm{f}}, \tag{2}$$

$$\hat{\mathcal{H}}_{\mathrm{b}} = -t_{\mathrm{b}} \sum_{\langle ij \rangle} \hat{b}_{i}^{\dagger} \hat{b}_{j} + \frac{U_{\mathrm{b}}}{2} \sum_{i} \hat{n}_{i}^{\mathrm{b}} (\hat{n}_{i}^{\mathrm{b}} - 1) - \left(2\mu - \delta - \frac{3\hbar\omega}{2}\right) \sum_{i} \hat{n}_{i}^{\mathrm{b}}, \tag{3}$$

$$\hat{\mathcal{H}}^0_{\rm fb} = U_{\rm fb}\sum_i \hat{n}^{\rm b}_i \hat{n}^{\rm f}_{i,0} + g_0 \sum_i (\hat{b}^\dagger_i \hat{c}_{i\uparrow,0}\hat{c}_{i\downarrow,0} + {\rm h.c.}), \tag{4}$$

$$\hat{\mathcal{H}}^l_{\rm f} = \sum_i \left(\left(2l + \frac{3}{2}\right)\hbar\omega - \mu\right)\hat{n}^{\rm f}_{i,l}, \tag{5}$$

$$\hat{\mathcal{H}}^l_{\rm fb} = g_l \sum_i (\hat{b}^\dagger_i \hat{c}_{i\uparrow,l}\hat{c}_{i\downarrow,l} + {\rm h.c.}), \tag{6}$$

where $\hat{c}^\dagger_{i\sigma,l}$ is the creation operator of a fermion with spin σ for the lth band on lattice site i. $\hat{b}^\dagger_i$ is the creation operator of a boson at site i. $\hat{n}^{\rm f}_{i\sigma,l} = \hat{c}^\dagger_{i\sigma,l}\hat{c}_{i\sigma,l}$ and $\hat{n}^{\rm f}_{i,l} = \hat{n}_{i\uparrow,l} + \hat{n}_{i\downarrow,l}$ are the fermionic number operators, and $\hat{n}^{\rm b}_i = \hat{b}^\dagger_i \hat{b}_i$ is the bosonic number operator. $t_{\rm f}$ and $t_{\rm b}$ are the tunneling amplitudes for fermions and bosons, respectively. $U_{\rm f}$, $U_{\rm b}$ and $U_{\rm fb}$ are the Fermi–Hubbard-, Bose–Hubbard and Bose–Fermi–Hubbard interactions, respectively. These interactions arise due to the background scattering lengths. Furthermore, μ is the chemical potential, δ is the detuning of the bosonic level and ω is the frequency of the harmonic oscillator associated with an optical lattice well. Finally, $g_l = g_0\sqrt{L^{(1/2)}_l(0)}$ is the Feshbach coupling to the lth band of the lattice, where g_0 is the Feshbach coupling for the lowest Hubbard band and $L^{(1/2)}_l(0)$ is the generalized Laguerre polynomial. Choosing the Feshbach couplings in this way guarantees that the two-body physics associated with the Feshbach resonance is incorporated exactly [35, 42].

The parameters of the generalized Hubbard Hamiltonian (1) are given by:

$$t_{\rm b(f)} \simeq \frac{4}{\sqrt{\pi}} E^{\rm b(f)}_{\rm r}\left(\frac{V_0}{E^{\rm b(f)}_{\rm r}}\right)^{3/4} \exp\left[-2\sqrt{\frac{V_0}{E^{\rm b(f)}_{\rm r}}}\right], \tag{7}$$

$$U_{\rm b(f)} \simeq \sqrt{\frac{8}{\pi}} k a_{\rm b(f)} E^{\rm b(f)}_{\rm r}\left(\frac{V_0}{E^{\rm b(f)}_{\rm r}}\right)^{3/4}, \tag{8}$$

$$U_{\rm fb} \simeq \frac{4}{\sqrt{\pi}} k a_{\rm fb} E^{\rm b}_{\rm r}\frac{1 + m_{\rm b}/m_{\rm f}}{(1+\sqrt{m_{\rm b}/m_{\rm f}})^{3/2}}\left(\frac{V_0}{E^{\rm b}_{\rm r}}\right)^{3/4}, \tag{9}$$

$$g = \hbar\sqrt{\frac{4\pi a_{\rm f}\Delta B \Delta\mu_{\rm mag}}{m_{\rm f}}}\left(\frac{m_{\rm f}\omega}{2\pi\hbar}\right)^{3/4}, \tag{10}$$

$$\delta = \Delta\mu_{\rm mag}(B - B_0). \tag{11}$$

Here, $E^{\rm f(b)}_{\rm r} = h^2/2\lambda^2 m_{\rm f(b)}$ is the recoil energy, V_0 is the amplitude of the optical lattice potential and λ is the laser wavelength. $a_{\rm f}$, $a_{\rm b}$ and $a_{\rm fb}$ are the fermion–fermion, boson–boson and fermion–boson background scattering lengths. In our calculation, we approximate the background boson–boson and the Bose–Fermi scattering lengths by $a_{\rm b} = 0.6a_{\rm f}$ [43] and $a_{\rm fb} = 1.2a_{\rm f}$ [44]. Furthermore, B is the magnetic field, and B_0 and ΔB are the position of the Feshbach resonance and its width, respectively. $\Delta\mu_{\rm mag}$ is the difference in the magnetic moment between

the closed and open channels of the Feshbach resonance. Finally, m_f and m_b are the respective masses of the fermions and bosons.

The Hamiltonian (1) can be simplified by the following rescaling:

$$\bar{\mu} = \mu - \frac{3\hbar\omega}{2}, \tag{12}$$

$$\bar{\delta} = \delta - \frac{3\hbar\omega}{2}, \tag{13}$$

such that the factor $3\hbar\omega/2$ disappears.

3. Method

3.1. Derivation of the effective single-band Hamiltonian

The multi-band Hamiltonian derived so far is very complicated, since it involves both strong correlations and many bands. Simply neglecting the higher bands would lead to an incorrect description close to the Feshbach resonance, since the Feshbach parameter g is very large and even exceeds the band gap [35]. However, the filling of fermions in the higher bands is strongly suppressed by the band gap. This allows us to perform a mean-field decoupling in the higher bands [35]. The lowest band is left untouched in this procedure since the fermionic filling can be large there.

We thus perform the following decoupling for $l > 0$ on each site:

$$\hat{\mathcal{H}}^{li}_\mathrm{fb} = g_l(\langle\hat{b}^\dagger_i\rangle\hat{c}_{i\uparrow,l}\hat{c}_{i\downarrow,l} + \hat{b}^\dagger_i\langle\hat{c}_{i\uparrow,l}\hat{c}_{i\downarrow,l}\rangle + \mathrm{h.c.}). \tag{14}$$

This step implies that the lowest band and the higher bands are only coupled in a mean-field way. They can thus be diagonalized separately, but are coupled by the mean-field self-consistency relations. The full Hamiltonian is now given by

$$\hat{\mathcal{H}} = \hat{\mathcal{H}}^0_\mathrm{f} + \hat{\mathcal{H}}_\mathrm{b} + \hat{\mathcal{H}}^0_\mathrm{fb} + \sum_i \hat{\mathcal{H}}'_b(i) + \sum_{l,i}\hat{\mathcal{H}}^{li}_\mathrm{fb}\,, \tag{15}$$

where the following terms are added to the bosonic part of the lowest band Hamiltonian:

$$\hat{\mathcal{H}}'_b(i) = \sum_{l=1} g_l(\hat{b}^\dagger_i\langle\hat{c}_{i\uparrow,l}\hat{c}_{i\downarrow,l}\rangle + \mathrm{h.c.}) = -(\Delta\hat{b}^\dagger_i + \mathrm{h.c.}), \tag{16}$$

where the mean-field Δ has been defined as $\Delta = -\sum_{l=1}^{\infty} g_l\langle\hat{c}_{i\uparrow,l}\hat{c}_{i\downarrow,l}\rangle$. For each of the higher bands $l > 0$ we obtain the following Hamiltonian (here we suppress the site index i):

$$\hat{\mathcal{H}}^l_\mathrm{f} = \begin{pmatrix}\hat{c}^\dagger_{l\uparrow} \\ \hat{c}_{l\downarrow}\end{pmatrix}\begin{pmatrix}2l\hbar\omega - \bar{\mu} & -g_l\langle\hat{b}\rangle \\ -g_l\langle\hat{b}^\dagger\rangle & -(2l\hbar\omega - \bar{\mu})\end{pmatrix}\begin{pmatrix}\hat{c}_{l\uparrow} \\ \hat{c}^\dagger_{l\downarrow}\end{pmatrix}. \tag{17}$$

The system described by equations (15)–(17) needs to be solved self-consistently with respect to the mean fields $\langle\hat{b}\rangle$ and Δ.

To diagonalize the Hamiltonian (17), one has to perform the following Bogoliubov transformation:

$$\begin{pmatrix}u_l & -v_l \\ v_l & u_l\end{pmatrix}\begin{pmatrix}2l\hbar\omega - \bar{\mu} & -g_l\langle\hat{b}\rangle \\ -g_l\langle\hat{b}^\dagger\rangle & -(2l\hbar\omega - \bar{\mu})\end{pmatrix}\begin{pmatrix}u_l & -v_l \\ v_l & u_l\end{pmatrix}^{-1} = \begin{pmatrix}-\omega_l & 0 \\ 0 & w_l\end{pmatrix}, \tag{18}$$

where

$$\omega_l = \sqrt{(2l\hbar\omega - \bar{\mu})^2 + g_l^2 |\langle \hat{b} \rangle|^2}, \tag{19}$$

$$u_l^2 = \frac{1}{2} + \frac{2l\hbar\omega - \bar{\mu}}{2\omega_l}, \tag{20}$$

$$v_l^2 = \frac{1}{2} - \frac{2l\hbar\omega - \bar{\mu}}{2\omega_l}, \tag{21}$$

$$u_l v_l = \frac{g_l \langle \hat{b} \rangle}{2\omega_l}. \tag{22}$$

This leads to the following expectation values:

$$n_l^F = 2v_l^2 + 2(u_l^2 - v_l^2) f(\omega_l) = 1 - \frac{2l\hbar\omega - \bar{\mu}}{\omega_l} \tanh\left(\frac{\omega_l}{2kT}\right), \tag{23}$$

$$|\langle \hat{c}_{l\uparrow} \hat{c}_{l\downarrow} \rangle| = |u_l v_l| \tanh\left(\frac{\omega_l}{2kT}\right) = \left| \frac{g_l \langle \hat{b} \rangle}{2\omega_l} \right| \tanh\left(\frac{\omega_l}{2kT}\right), \tag{24}$$

where $f(\omega_l)$ is the Fermi function and T is the temperature. We use absolute values in the equation for $\langle \hat{c}_{l\uparrow} \hat{c}_{l\downarrow} \rangle$ because of the ambiguity of the sign, which arise from the fact that still a divergence has to be subtracted (see below).

The total number of fermions is equal to

$$n_{\text{tot}}^{\text{F}} = n_0^{\text{F}} + \sum_{l=1}^{\infty} \left(1 - \frac{2l\hbar\omega - \bar{\mu}}{\omega_l} \tanh\left(\frac{\omega_l}{2kT}\right) \right). \tag{25}$$

This is a converging sum, which can be evaluated numerically.

From equation (16) it follows that we have to evaluate the sum

$$\sum_{l=1} g_l \langle \hat{c}_{l\uparrow} \hat{c}_{l\downarrow} \rangle = \pm \langle \hat{b} \rangle \sum_{l=1} \frac{g_l^2}{2\omega_l} \tanh\left(\frac{\omega_l}{2kT}\right), \tag{26}$$

which is divergent. This divergence always arises in the gap equation of the BCS model when the T-matrix is approximated by a delta-potential [35, 42]. One way to solve this problem is by using a pseudo-potential instead of the delta-potential [42]. Here, however, we follow [35] and explicitly isolate the diverging contribution from the sum.

First, we note that for large l, ω_l can be approximated by $\omega_l = 2l\hbar\omega - \bar{\mu}$ and $\tanh(\omega_l/2kT) \simeq 1$. Therefore

$$\begin{aligned} \sum_{l=1} \frac{g_l^2}{2\omega_l} \tanh\left(\frac{\omega_l}{2kT}\right) &\simeq \left(\sum_{l=1}^{N} \frac{g_l^2}{2\omega_l} \tanh\left(\frac{\omega_l}{2kT}\right) + \sum_{l=N+1}^{\infty} \frac{g_l^2}{2(2l\hbar\omega - \bar{\mu})} \right) \\ &= \left(\sum_{l=1}^{N} \frac{g_l^2}{2\omega_l} \tanh\left(\frac{\omega_l}{2kT}\right) - \sum_{l=0}^{N} \frac{g_l^2}{2(2l\hbar\omega - \bar{\mu})} + \sum_{l=0}^{\infty} \frac{g_l^2}{2(2l\hbar\omega - \bar{\mu})} \right). \end{aligned} \tag{27}$$

Here, N is a large integer (in our calculation we took $N = 500$).

The first two terms of equation (27) are finite sums, but the last term diverges. This sum is known from the literature [42, 45]. To separate the diverging part, we have to take the following limit:

$$\sum_{l=0}^{\infty} \frac{g_l^2}{2(2l\hbar\omega - \bar{\mu})} = \sum_{l=0}^{\infty} \frac{g_0^2 L_l^{(1/2)}(0)}{2(2l\hbar\omega - \bar{\mu})} = \lim_{r\to 0} \sum_{l=0}^{\infty} \frac{g_0^2 L_l^{(1/2)}(r)}{2(2l\hbar\omega - \bar{\mu})}$$
$$= -\lim_{r\to 0} \left(\frac{g_0^2 \sqrt{\pi}\,\Gamma(-\bar{\mu}/2\hbar\omega)/\,\Gamma(-\bar{\mu}/2\hbar\omega - 1/2)}{2\hbar\omega} - \frac{\sqrt{\pi}}{r} + \mathcal{O}(r) \right). \tag{28}$$

Since the diverging part $\sqrt{\pi}/r$ is independent of the model parameters, we can cure the divergence by neglecting this term [35, 42]. Doing so, we obtain

$$\Delta = -\sum_{l=1}^{\infty} g_l \langle \hat{c}_{l\uparrow} \hat{c}_{l\downarrow} \rangle = \pm \langle \hat{b} \rangle \left(\frac{g_0^2 \sqrt{\pi}\,\Gamma(-\bar{\mu}/\hbar\omega)/\,\Gamma(-\bar{\mu}/\hbar\omega - 1/2)}{2\hbar\omega} \right.$$
$$\left. + \sum_{l=0}^{N} \frac{g_l^2}{2(2l\hbar\omega - \bar{\mu})} - \sum_{l=1}^{N} \frac{g_l^2}{2\omega_l} \tanh\left(\frac{\omega_l}{2kT}\right) \right). \tag{29}$$

We now fix the sign by requiring $\Delta > 0$, since this solution minimizes the (free) energy.

Summarizing, we have reduced the multi-band problem to an effective single-band Hamiltonian:

$$\hat{\mathcal{H}} = \hat{\mathcal{H}}_f^0 + \hat{\mathcal{H}}_\mathrm{b} + \hat{\mathcal{H}}_\mathrm{b}' + \hat{\mathcal{H}}_\mathrm{fb}^0, \tag{30}$$

where $\hat{\mathcal{H}}_\mathrm{f}^0$, $\hat{\mathcal{H}}_\mathrm{b}$, $\hat{\mathcal{H}}_\mathrm{fb}^0$ and $\hat{\mathcal{H}}_\mathrm{b}'$ are given by equations (2), (3), (4) and (16), respectively.

The chemical potential μ has to be adjusted such that the total filling is equal to the desired value n_tot:

$$2n_0^\mathrm{b} + n_0^\mathrm{F} + \sum_{l=1}^{\infty} \left(1 - \frac{2l\hbar\omega - \bar{\mu}}{\omega_l} \tanh\left(\frac{\omega_l}{2kT}\right) \right) = n_\mathrm{tot}. \tag{31}$$

This leads to the following self-consistency loop: we start from an initial guess of the superfluid order parameter $\langle \hat{b} \rangle$ and calculate Δ using equation (29). As a result, we know all parameters in the Hamiltonian (30), and we can find its eigenvalues and eigenvectors and correspondingly calculate new correlation functions, including the superfluid order parameter $\langle \hat{b} \rangle$. With this step, the self-consistency loop is closed.

It is worth noting that the effective single-band Hamiltonian we have derived here is different from the effective single-band model in terms of the dressed particles derived in other approaches [36, 39]: the bosons and fermions in our Hamiltonian correspond to the bare particles in the lowest band.

3.2. GDMFT

To analyze the Hamiltonian (30), we use GDMFT that is explained in detail in [27, 28]. Here we only mention that within GDMFT one considers a single site that is self-consistently coupled to a dynamical fermionic bath corresponding to DMFT [29, 30] and a static bosonic mean-field corresponding to bosonic Gutzwiller [31–33]. These are the leading order contributions in a

$1/z$-expansion of the effective action (z being the lattice coordination number). Hence GMDFT is exact in infinite dimensions and is expected to be a good approximation for the cubic lattice considered here, for which $z = 6$. The typical accuracy for low-temperature expectation values is around 20%.

In the specific case considered here, the system is described by a generalized single-impurity Anderson model (GSIAM) with the following Anderson Hamiltonian:

$$\begin{aligned}
\hat{\mathcal{H}}^{\mathrm{And}} &= \hat{\mathcal{H}}^{\mathrm{And}}_{\mathrm{f}} + \hat{\mathcal{H}}^{\mathrm{And}}_{\mathrm{fb}} + \hat{\mathcal{H}}^{\mathrm{And}}_{\mathrm{b}}, \\
\hat{\mathcal{H}}^{\mathrm{And}}_{\mathrm{b}} &= -[(zt_{\mathrm{b}}\varphi \ + \Delta)\hat{b}^{\dagger} + \mathrm{h.c.}] + \frac{U_{\mathrm{b}}}{2}\hat{n}^{\mathrm{b}}(\hat{n}^{\mathrm{b}} - 1) - (2\bar{\mu} - \bar{\delta})\hat{n}^{\mathrm{b}}, \\
\hat{\mathcal{H}}^{\mathrm{And}}_{\mathrm{fb}} &= U_{\mathrm{fb}}\hat{n}^{\mathrm{f}}\hat{n}^{\mathrm{b}} + g_0(\hat{b}_i^{\dagger}\hat{c}_{\uparrow}\hat{c}_{\downarrow} + \mathrm{h.c.}), \\
\hat{\mathcal{H}}^{\mathrm{And}}_{\mathrm{f}} &= -\bar{\mu}\hat{n}^{\mathrm{f}} + U_{\mathrm{f}}\hat{n}^{\mathrm{f}}_{\uparrow}\hat{n}^{\mathrm{f}}_{\downarrow} + \sum_{k,\sigma}\{\varepsilon_k\hat{a}^{\dagger}_{k\sigma}\hat{a}_{k\sigma} + V_k(\hat{c}^{\dagger}_{\sigma}\hat{a}_{k\sigma} + \mathrm{h.c.})\} + \sum_{k} W_k(\hat{a}^{\dagger}_{k\uparrow}\hat{a}^{\dagger}_{k\downarrow} + \mathrm{h.c.}),
\end{aligned} \tag{32}$$

where z is the lattice coordination number and $\varphi = \langle\hat{b}\rangle$ is the superfluid order parameter. k labels the noninteracting orbitals of the effective bath, V_k are the corresponding fermionic hybridization matrix elements, W_k describes the superfluid properties of the bath and $a^{\dagger}_{k\sigma}$ is the creation operator of a fermion in the kth orbital of the bath with spin σ. $\hat{n}_{\mathrm{f}\sigma} = \hat{c}^{\dagger}_{\sigma}c_{\sigma}$ is the fermionic number operator and $\hat{n} = \hat{n}_{\mathrm{f}\uparrow} + \hat{n}_{\mathrm{f}\downarrow}$.

To solve the Anderson Hamiltonian, we use exact diagonalization as the impurity solver [46–49]. In this algorithm, the infinite number of orbitals in Hamiltonian (32) is truncated and only a finite number of n_{s} orbitals is considered. The resulting finite-size problem is fundamentally different from the finite-size problem of a finite number of lattice sites of the original Hubbard model, and the truncation procedure can be viewed using a finite number of parameters (energy scales) to describe the local dynamics encoded in the Weiss Green's function:

$$\mathcal{G}^{-1}_{\mathrm{And}}(\mathrm{i}\omega_n) = \mathcal{G}^{-1}_{\sigma,\mathrm{And}}(\mathrm{i}\omega_n) = \mathrm{i}\omega_n + \bar{\mu} + \sum_{l=1}^{n_{\mathrm{s}}} V^2_{l\sigma}\frac{\mathrm{i}\omega_n + \varepsilon_l}{\varepsilon_l^2 + \omega_n^2 + W_l^2}, \tag{33}$$

$$\mathcal{F}^{-1}_{\mathrm{And}}(\mathrm{i}\omega_n) = \sum_{l=1}^{n_{\mathrm{s}}}\frac{V_l^2 W_l}{\varepsilon_l^2 + \omega_n^2 + W_l^2}, \tag{34}$$

where β is the inverse temperature and $\omega_n = (2n+1)\pi/\beta$ are the Matsubara frequencies.

To close the self-consistency loop by using the lattice Dyson equation, we calculate the normal and superfluid Green's functions, which can be written as follows [46]:

$$G(\mathrm{i}\omega_n) = G_{\sigma}(\mathrm{i}\omega_n) = \int_{-\infty}^{\infty}\mathrm{d}\varepsilon\, D(\varepsilon)\frac{\zeta^* - \varepsilon}{|\zeta - \varepsilon|^2 + \Sigma^2_{\mathrm{SC}}}, \tag{35}$$

$$F(\mathrm{i}\omega_n) = -\Sigma_{\mathrm{SC}}(\mathrm{i}\omega_n)\int_{-\infty}^{\infty}\mathrm{d}\varepsilon\, D(\varepsilon)\frac{1}{|\zeta - \varepsilon|^2 + \Sigma^2_{\mathrm{SC}}}, \tag{36}$$

where $\zeta = \mathrm{i}\omega_n + \bar{\mu} - \Sigma(\mathrm{i}\omega_n)$ and $D(\varepsilon)$ is the noninteracting density of states of the cubic lattice. $\Sigma(\mathrm{i}\omega_n)$ and $\Sigma_{\mathrm{SC}}(\mathrm{i}\omega_n)$ are the normal and superfluid self-energies, which as shown in

the appendix can be expressed via a set of higher-order Green's functions:

$$\Sigma(\mathrm{i}\omega_n) = \Sigma_\sigma(\mathrm{i}\omega_n) = \frac{(U_\mathrm{f} Q_{\mathrm{ff}\sigma}(\mathrm{i}\omega_n) + U_\mathrm{fb} Q_{\mathrm{fb}\sigma}(\mathrm{i}\omega_n) + \sigma g Q^*_{g\bar\sigma\sigma}(\mathrm{i}\omega_n)) G^*_{\bar\sigma}(\mathrm{i}\omega_n)}{G_\sigma(\mathrm{i}\omega_n) G^*_{\bar\sigma}(\mathrm{i}\omega_n) + F(\sigma\mathrm{i}\omega_n) F^*(\bar\sigma\mathrm{i}\omega_n)} + \frac{(\sigma U_\mathrm{f} Q_{\mathrm{ff},\sigma\bar\sigma}(\mathrm{i}\omega_n) + \sigma U_\mathrm{fb} Q_{\mathrm{fb}\sigma\bar\sigma}(\mathrm{i}\omega_n) + g Q^*_{g\bar\sigma}(\mathrm{i}\omega_n)) F^*(\bar\sigma\mathrm{i}\omega_n)}{G_\sigma(\mathrm{i}\omega_n) G^*_{\bar\sigma}(\mathrm{i}\omega_n) + F(\sigma\mathrm{i}\omega_n) F^*(\bar\sigma\mathrm{i}\omega_n)}, \tag{37}$$

$$\Sigma_\mathrm{SC}(\mathrm{i}\omega_n) = \frac{(U_\mathrm{f} Q_{\mathrm{ff}\uparrow}(\mathrm{i}\omega_n) + U_\mathrm{fb} Q_{\mathrm{fb}\uparrow}(\mathrm{i}\omega_n) + g Q^*_{g\downarrow\uparrow}(\mathrm{i}\omega_n)) F(\mathrm{i}\omega_n)}{G_\uparrow(\mathrm{i}\omega_n) G^*_\downarrow(\mathrm{i}\omega_n) + F(\mathrm{i}\omega_n) F^*(-\mathrm{i}\omega_n)} - \frac{(U_\mathrm{f} Q_{\mathrm{ff},\uparrow\downarrow}(\mathrm{i}\omega_n) + U_\mathrm{fb} Q_{\mathrm{fb}\uparrow\downarrow}(\mathrm{i}\omega_n) + g Q^*_{g\downarrow}(\mathrm{i}\omega_n)) G_\uparrow(\mathrm{i}\omega_n)}{G_\uparrow(\mathrm{i}\omega_n) G^*_\downarrow(\mathrm{i}\omega_n) + F(\mathrm{i}\omega_n) F^*(-\mathrm{i}\omega_n)}. \tag{38}$$

Here, $G(\mathrm{i}\omega_n) = \langle\langle c_{\sigma,0}, c^\dagger_{\sigma,0}\rangle\rangle_\omega$ and $F(\mathrm{i}\omega_n) = \langle\langle c_{\uparrow,0}, c_{\downarrow,0}\rangle\rangle_\omega$ are the normal and superfluid single-particle Green's functions. In addition, we have also defined the following additional interacting Green's functions: $Q_{\mathrm{ff}\sigma}(\mathrm{i}\omega_n) = \langle\langle \hat f_\sigma \hat f^\dagger_{\bar\sigma} \hat f_{\bar\sigma}, \hat f^\dagger_\sigma\rangle\rangle_\omega$, $Q_{\mathrm{ff}\sigma\bar\sigma}(\mathrm{i}\omega_n) = \langle\langle \hat f_\sigma \hat f^\dagger_{\bar\sigma} \hat f_{\bar\sigma}, \hat f_{\bar\sigma}\rangle\rangle_\omega$, $Q_{\mathrm{fb}\sigma}(\mathrm{i}\omega_n) = \langle\langle \hat f_\sigma \hat b^\dagger \hat b, \hat f^\dagger_\sigma\rangle\rangle_\omega$, $Q_{\mathrm{fb}\sigma\bar\sigma}(\mathrm{i}\omega_n) = \langle\langle \hat f_\sigma \hat b^\dagger \hat b, \hat f_{\bar\sigma}\rangle\rangle_\omega$, $Q_{g\sigma}(\mathrm{i}\omega_n) = \langle\langle \hat f_\sigma \hat b^\dagger, \hat f^\dagger_\sigma\rangle\rangle_\omega$ and $Q_{g\sigma\bar\sigma}(\mathrm{i}\omega_n) = \langle\langle \hat f_\sigma \hat b^\dagger, \hat f_{\bar\sigma}\rangle\rangle_\omega$. Here,

$$\langle\langle \hat A, \hat B\rangle\rangle_\omega = -\frac{1}{Z}\sum_{n,m} \langle n|\hat A|m\rangle\langle m|\hat B|n\rangle \frac{\mathrm{e}^{-\beta E_n} + \mathrm{e}^{-\beta E_m}}{E_m - E_n - \mathrm{i}\omega_n} \tag{39}$$

and

$$Z = \sum_n \mathrm{e}^{-\beta E_n} \tag{40}$$

is the partition function.

The relation between the Weiss field and the Green's function is given by the local Dyson equation:

$$\hat{\mathcal{G}}^{-1}_\mathrm{ex}(\mathrm{i}\omega_n) = \hat\Sigma(\mathrm{i}\omega_n) + \hat G^{-1}(\mathrm{i}\omega_n), \tag{41}$$

where

$$\hat G(\mathrm{i}\omega_n) = \begin{pmatrix} G(\mathrm{i}\omega_n) & F(\mathrm{i}\omega_n) \\ F(\mathrm{i}\omega_n) & -G^*(\mathrm{i}\omega_n) \end{pmatrix} \tag{42}$$

is the matrix of interacting Green's functions,

$$\hat\Sigma(\mathrm{i}\omega_n) = \begin{pmatrix} \Sigma(\mathrm{i}\omega_n) & \Sigma_\mathrm{SC}(\mathrm{i}\omega_n) \\ \Sigma_\mathrm{SC}(\mathrm{i}\omega_n) & -\Sigma^*(\mathrm{i}\omega_n) \end{pmatrix} \tag{43}$$

is the self-energy matrix and

$$\hat{\mathcal{G}}_\mathrm{ex}(\mathrm{i}\omega_n) = \begin{pmatrix} \mathcal{G}_\mathrm{ex}(\mathrm{i}\omega_n) & \mathcal{F}_\mathrm{ex}(\mathrm{i}\omega_n) \\ \mathcal{F}_\mathrm{ex}(\mathrm{i}\omega_n) & -\mathcal{G}^*_\mathrm{ex}(\mathrm{i}\omega_n) \end{pmatrix} \tag{44}$$

is the matrix of Weiss Green's functions.

To determine new parameters for the Anderson Hamiltonian, we fit the Weiss functions calculated from (33) and (34) to the ones calculated from the eigenstates of the Anderson Hamiltonian via the local Dyson equation (41). We use a steepest descent method with the following norm:

$$\chi = \frac{1}{2(N_{\max}+1)} \sum_{n=0}^{N_{\max}} \frac{1}{2n+1} \left(|\mathcal{G}^{-1}_{\mathrm{And}}(\mathrm{i}\omega_n) - \mathcal{G}^{-1}_{\mathrm{ex}}(\mathrm{i}\omega_n)|^2 + |\mathcal{F}^{-1}_{\mathrm{And}}(\mathrm{i}\omega_n) - \mathcal{F}^{-1}_{\mathrm{ex}}(\mathrm{i}\omega_n)|^2 \right), \tag{45}$$

where $N_{\max}$ is the number of Matsubara frequencies taken into account.

The minimization procedure works as follows. We start from an initial guess of the GSIAM parameters ($\epsilon_{l\sigma}$, $V_{l\sigma}$ and W_l), and then, knowing the local Green's functions calculated from equation (39) and the self-energies calculated from (37) and (38), we calculate the lattice Green's function according to equations (35) and (36). Subsequently, using the Dyson equation (41) we can calculate the Weiss Green's functions $\mathcal{G}^{-1}_{\sigma,\mathrm{ex}}(\mathrm{i}\omega_n)$ and $\mathcal{F}^{-1}_{\sigma,\mathrm{ex}}(\mathrm{i}\omega_n)$. The next step is to fit this result by the parameterization in equations (33) and (34) and thus to find a new set of parameters for the GSIAM. These new parameters serve as input for the next iteration. This procedure is repeated until convergence is reached.

3.3. Calculation of the critical temperature

The combination of the mean-field approximation in the higher bands and GDMFT explained so far, however, leads to a problem. Both approximations involve the superfluid order parameter $\langle \hat{b}_i \rangle$. The mean-field approximation for the higher bands implies that the local correlator $\langle \hat{b}_i^\dagger \hat{c}_{i\uparrow,l} \hat{c}_{i\downarrow,l} \rangle$ is approximated by $\langle \hat{b}_i^\dagger \rangle \langle \hat{c}_{i\uparrow,l} \hat{c}_{i\downarrow,l} \rangle$. The GDMFT scheme, on the other hand, involves the approximation to replace the nonlocal correlator $\langle \hat{b}_i^\dagger \hat{b}_j \rangle$ by $\langle \hat{b}_i^\dagger \rangle \langle \hat{b}_j \rangle$. This means that $\langle \hat{b} \rangle$ both measures the local phase coherence between bosons and fermions and the nonlocal bosonic long-range order. However, these are two very different quantities that generally cannot be described by a single mean-field order parameter. At zero temperature, this problem is not very severe, because in this case one expects both long-range order and on-site boson–fermion coherence, so that $\langle \hat{b} \rangle$ is large for both reasons. At finite temperature, however, this becomes a real problem, because the bosonic long range order is expected to vanish at temperatures of the order of the bosonic hopping t_{b}. The local boson–fermion coherence, on the other hand, persists for much higher temperatures, since the coupling g is orders of magnitude larger than t_{b}. Indeed, we find that, in the approximation outlined above, the full GDMFT calculations are in good agreement with a single-site approximation. In the single-site approach, the impurity site couples neither to the fermionic nor to the bosonic bath and long-range order cannot be inferred. The critical temperature obtained from this calculation can be identified with the pair breaking temperature T_{pair}, which is much higher than the relevant temperature in experiments.

The scheme explained in the previous subsection cannot therefore be used to infer the critical temperature for superfluid long-range order. In order to do so, we have to modify the approximation and remove the ambiguous nature of the order parameter $\langle \hat{b} \rangle$. This is made possible by the observation that the term $\Delta \hat{b}^\dagger$ in the Hamiltonian merely renormalizes the self-energy of the bosons: in the BEC regime the bosons are in a coherent state and this term is equivalent to a shift of the bosonic chemical potential. This is also clear from the treatment in [35], where terms from higher bands enter the bosonic self-energy. To make this more explicit,

we write

$$\Delta = -\sum_{l=1}^{\infty} g_l \langle \hat{c}_{l\uparrow} \hat{c}_{l\downarrow} \rangle = \pm \langle \hat{b} \rangle \left(\frac{g_0^2 \sqrt{\pi} \Gamma(-\bar{\mu}/\hbar\omega) / \Gamma(-\bar{\mu}/\hbar\omega - 1/2)}{2\hbar\omega} + \sum_{l=0}^{N} \frac{g_l^2}{2(2l\hbar\omega - \bar{\mu})} - \sum_{l=1}^{N} \frac{g_l^2}{2\omega_l} \tanh\left(\frac{\omega_l}{2kT}\right) \right) \equiv \langle \hat{b} \rangle \Delta'. \tag{46}$$

We can therefore replace the term

$$-(\Delta \hat{b}^\dagger + \text{h.c.}) = -(\Delta' \langle \hat{b} \rangle \hat{b}^\dagger + \text{h.c.}) \tag{47}$$

in the Hamiltonian by

$$-\Delta' \hat{b}^\dagger \hat{b}\,, \tag{48}$$

such that terms from the higher bands only renormalize the chemical potential. We remark here that this might look like an additional approximation. However, one has to keep in mind that the term connecting Δ to the bosonic creation operator originated from the mean-field approximation in the higher bands. By treating the contribution of higher bands within the bosonic self-energy, we are therefore restoring part of the mean-field approximation made in the previous step. Indeed, by using second-order perturbation theory in the couplings to higher bands (which is justified if the band energy exceeds the Feshbach coupling), we can also obtain this correction directly as part of the bosonic self-energy, without invoking a mean-field decoupling.

This improved approximation for treating higher bands gives for $T = 0$ similar results as before; in particular the position of the transition to the Mott insulator is in good approximation the same. The superfluid order parameter is smaller, as expected. However, for nonzero temperatures, this improved approximation scheme allows for a calculation of the critical temperature for superfluid long-range order, which was not possible in the previous approximation.

4. Results

We study a mixture of potassium atoms (^{40}K) and Feshbach molecules in a 3D optical lattice. The on-site harmonic oscillator frequency is chosen to be $\omega = 2\pi \times 58275\,\text{Hz}$, which corresponds to a lattice with wavelength $\lambda = 806\,\text{nm}$ and a Rabi frequency of $\Omega_\text{R} = 2\pi \times 1.43\,\text{GHz}$. The Feshbach resonance considered here is at $B = 202.1\,\text{G}$ and the width of the resonance is 7.8 G [50]. The difference between the magnetic moments of the closed and open channels of the Feshbach resonance is $\Delta\mu = 16/9\mu_\text{B}$, where μ_B is the Bohr magneton. The total filling per lattice site in our calculation is $n_\text{tot} = 1$.

4.1. Zero temperature

First, we consider the case of zero temperature. Our calculations for the ground state are summarized in figure 2. Deep in the BEC regime only bosonic molecules are present. When the magnetic field is increased, close to resonance the number of fermions is increasing and the number of bosons decreasing. Above the resonance we mainly have fermions and the number of bosons is small. Both fermions and bosons are superfluid. We remark again that here we describe

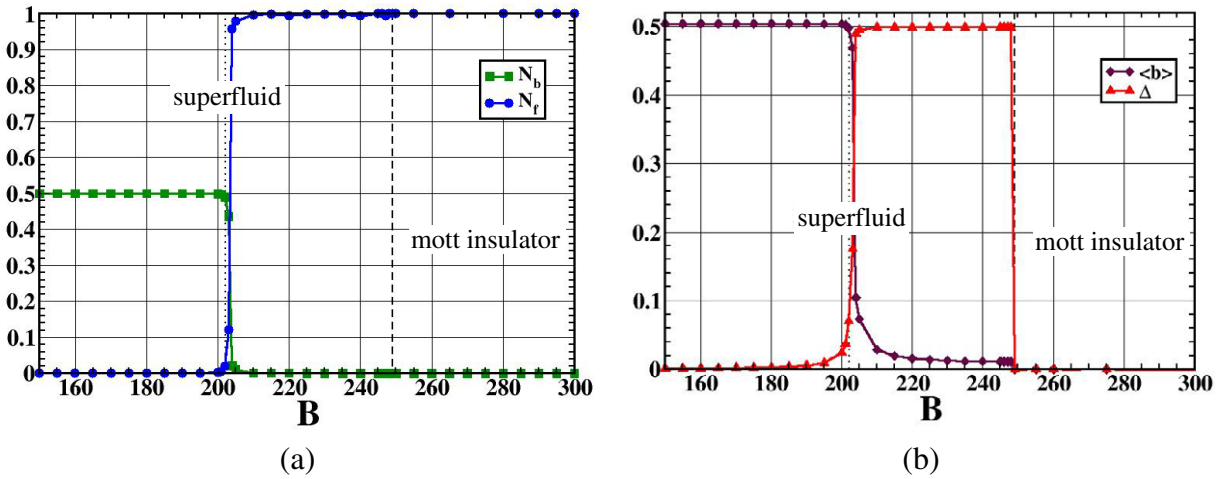

Figure 2. Bosonic and fermionic filling (a) and superfluid order parameters (b) as a function of magnetic field B for $T = 0$. The dotted line corresponds to the Feshbach resonance, whereas the dashed line indicates the phase transition from the superfluid phase to the Mott insulator phase. The magnetic field is measured in units of Gauss.

the physics in terms of bare bosons and fermions: in terms of dressed particles as in [35], these are still molecular bosons and the BEC–BCS crossover takes place when the bosonic self-energy crosses twice the Fermi energy [35]. However, in the case of half-filled fermions, this crossover is intercepted by a first-order phase transition to a fermionic Mott insulator state, which happens at a critical value of the magnetic field of $B = 249\,\mathrm{G}$. Calculations that include only the lowest band of the Bose–Fermi–Hubbard model (as well as with one and two excited bands) yield this transition to the Mott insulator phase already close to the Feshbach resonance at $B \simeq 205\,\mathrm{G}$ (results not shown). This implies that, to capture the superfluid region $205\,\mathrm{T} \lesssim B < 249\,\mathrm{T}$, higher bands that renormalize the bosonic self-energy are crucial.

Another point worth noting is the first-order nature of the transition to the Mott insulating state. In contrast, if one integrates out the bosonic degree of freedom and describes the Feshbach resonance in terms of an effective, attractive interaction between the fermions within a single-channel model for the lowest band, one finds a different scenario. In this case, the induced attractive interaction dominates, until it is cancelled by the repulsive background interaction. This means that within the single-channel approximation, one finds a regime with a normal Fermi-liquid phase in between the BEC/BCS phase and the Mott insulator, which is absent in our phase diagram. This directly indicates that the effect of higher bands is crucial to capture the first-order transition between the superfluid and insulator phases.

4.2. Nonzero temperature

Having clarified the ground state phase diagram, we now consider finite temperature. In particular, we investigate the critical temperature for the transition to the normal state. Deep in the BEC regime, the critical temperature is constant ($T_c \approx 0.21 t_f$) and completely determined by the properties of the bosons: the bosonic hopping parameter t_b, the interbosonic background scattering length a_b and the bosonic density. Only very close to resonance the

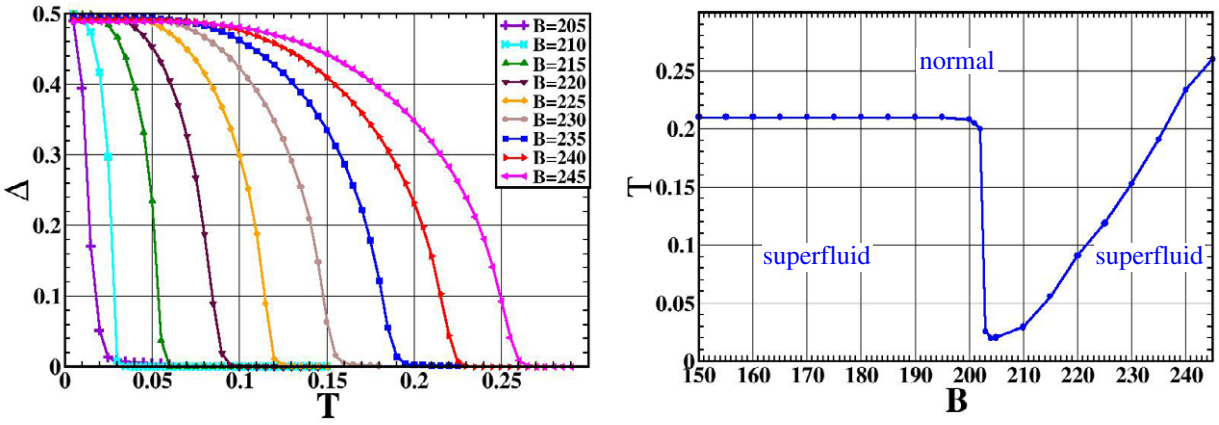

Figure 3. Finite temperature results. In (a) we plot the fermionic superfluid order parameter as a function of temperature T for different magnetic fields above the resonance. In (b) we show the phase diagram. The blue solid line separates the superfluid phase from the normal phase. Here temperature is measured in units of the fermionic hopping t_f.

critical temperature suddenly drops (see figure 3). This coincides with the magnetic field value for which fermions enter the system. On the BCS side of the resonance, the critical temperature depends on the magnetic field and increases with B (see figure 3). This implies that at resonance the critical temperature is *minimal*. This is in sharp contrast to the situation where no lattice is present, in which case the critical temperature is *maximal* close to resonance.

This surprising fact can be understood from the behavior of the critical temperature in the single-band attractive Hubbard model [51, 52]. In this model, the critical temperature is low for both very large and very small attraction and has a maximum in between. The reason for the low critical temperature at small attraction is the conventional exponential suppression of T_c in the BCS regime. For strong attraction the critical temperature decreases again because the fermions start forming bound pairs with a greatly enhanced effective mass. Identifying the resonance position with the case of very large attraction, this explains the low critical temperature at this point. When moving away from resonance, the effective attraction induced by the Feshbach resonance becomes weaker and hence the critical temperature increases again. Far away from resonance one would therefore expect to find a maximum of the critical temperature, after which it decreases again because the BCS regime of weak attraction is entered. However, due to the transition into the Mott insulator phase for the unit filling considered here, we cannot see the maximum of the critical temperature. Estimating the induced attractive interaction at the transition point to the Mott insulator by assuming it to be equal to the repulsive background interaction, this indeed gives a value for the induced attractive interaction that is larger (in absolute value) than the position of the maximum in the single-band attractive Hubbard model [51, 52].

Our calculation also shows that, on both sides of the resonance, the ratio $\langle c_\uparrow c_\downarrow \rangle / \langle b^\dagger \rangle$ as a function of the temperature for fixed values of the magnetic field is constant. This means that the on-site Bose–Fermi coherence is not affected by the temperature for the low temperatures considered here.

5. Summary

We have studied ultracold fermionic ^{40}K atoms in a 3D optical lattice close to a Feshbach resonance. We derived an effective description in terms of a Bose–Fermi–Hubbard model, in which the molecular degree of freedom is explicitly present. Our calculations show, in agreement with [35], that the effect of higher bands is crucial for a correct description of the Feshbach physics. We therefore take into account the fermionic occupation of higher bands.

To solve the strongly interacting multi-band problem, we decouple the higher bands from the lowest one via a mean-field decoupling and reduce the Hamiltonian to an effective single-band Bose–Fermi–Hubbard model, which is self-consistently coupled to the higher bands. To solve this resulting model we use GDMFT.

The low-temperature physics close to the Feshbach resonance is very rich. Upon changing the magnetic field, the ratio of fermionic and bosonic densities changes. Below the resonance the system is mainly occupied by molecular bosons forming a condensate. Close to resonance the number of bosons decreases, whereas the number of fermions increases. The fermions are in the superfluid phase. This resembles the BEC–BCS crossover close to a Feshbach resonance without an optical lattice. In addition, for the unit total filling considered here, we found a transition into the fermionic Mott insulator phase when the magnetic field is increased even further. The Mott insulator phase is stabilized by the repulsive fermionic background scattering, which at large magnetic fields overcomes the attractive interaction induced by the Feshbach resonance. The phase transition into the Mott insulator is found to be of first order. We found that higher bands are crucial for a quantitatively correct prediction of the transition point.

We also calculated the critical temperature of the BEC/BCS superfluid phase across the resonance. Below resonance the critical temperature is independent of the magnetic field, until it sharply drops close to resonance. Above the resonance the critical temperature increases again, leading to the remarkable result of a *minimal* critical temperature at resonance.

Acknowledgments

We thank H T C Stoof and A Koetsier for useful discussions. This work was supported by the German Research Foundation (DFG) through grant number HO 2407/2-1, Collaborative Research Center (SFB/TR 49) and Nederlandse Organisatie voor Wetenschappelijk Onderzoek (NWO).

Appendix. Derivation of the self-energy for the Bose–Fermi mixture

In this appendix, we evaluate the self-energy via correlation functions. For this purpose, we use the equation of motion, which in general has the following form:

$$\mathrm{i}\omega_n \langle\langle \hat{A}, \hat{B}\rangle\rangle_\omega + \langle\langle [\hat{\mathcal{H}}, \hat{A}]_-, \hat{B}\rangle\rangle_\omega = \langle [\hat{A}, \hat{B}]_\eta \rangle. \tag{A.1}$$

Here, ω_n are the Matsubara frequencies and $\langle\langle \hat{A}, \hat{B}\rangle\rangle_\omega$ is the general form of the Green's function, with the usual notation $[\hat{A}, \hat{B}]_\pm \equiv \hat{A}\hat{B} \pm \hat{B}\hat{A}$; the plus sign applies when both operators are fermionic; otherwise the minus sign is used.

For the resonantly interacting Bose–Fermi mixture, the generalized single-impurity Anderson Hamiltonian has the following form:

$$\hat{\mathcal{H}}^{\mathrm{And}} = -\sum_{\sigma} \mu_{f\sigma} \hat{n}^{\mathrm{f}}_{\sigma} + U_{\mathrm{f}} \hat{n}^{\mathrm{f}}_{\uparrow} \hat{n}^{\mathrm{f}}_{\downarrow} + U_{\mathrm{fb}} \hat{n}^{\mathrm{f}} \hat{n}^{\mathrm{b}} + g(\hat{f}^{\dagger}_{\downarrow} \hat{f}^{\dagger}_{\uparrow} \hat{b} + \mathrm{h.c.}) + \hat{\mathcal{H}}^{\mathrm{And}}_{\mathrm{b}} + \sum_{k\sigma} V_{k\sigma} (\hat{f}^{\dagger}_{\sigma} \hat{c}_{k\sigma} + \mathrm{h.c.}) + \sum_{k\sigma} \varepsilon_{k\sigma} \hat{c}^{\dagger}_{k\sigma} \hat{c}_{k\sigma} + \sum_{k} W_k (\hat{c}^{\dagger}_{k\uparrow} \hat{c}^{\dagger}_{k\downarrow} + \mathrm{h.c.}), \tag{A.2}$$

where $\hat{f}^{\dagger}_{\sigma}$ and $\hat{c}^{\dagger}_{k\sigma}$ are the fermionic creation operators on the 'impurity site' and in the band, respectively. $\hat{b}^{\dagger}$ is the bosonic creation operator on the impurity site. $\hat{n}^{\mathrm{f}} = \hat{n}^{\mathrm{f}}_{\uparrow} + \hat{n}^{\mathrm{f}}_{\downarrow} = \sum_{\sigma} \hat{f}^{\dagger}_{\sigma} \hat{f}_{\sigma}$, $\hat{n}^{\mathrm{b}} = \hat{b}^{\dagger} \hat{b}$ and $\hat{\mathcal{H}}^{\mathrm{And}}_{\mathrm{b}}$ is the bosonic part of the Hamiltonian.

To calculate the self-energy, we first evaluate the following commutator relations:

$$[\hat{\mathcal{H}}^{\mathrm{And}}, \hat{f}_{\sigma}]_{-} = \mu_{f\sigma} \hat{f}_{\sigma} - U_{\mathrm{f}} \hat{f}_{\sigma} \hat{f}^{\dagger}_{\bar{\sigma}} \hat{f}_{\bar{\sigma}} - U_{\mathrm{fb}} \hat{f}_{\sigma} \hat{b}^{\dagger} \hat{b} + \sigma g \hat{f}^{\dagger}_{\bar{\sigma}} \hat{b} - \sum_{k} V_{k\sigma} \hat{c}_{k\sigma}, \tag{A.3}$$

$$[\hat{\mathcal{H}}^{\mathrm{And}}, \hat{f}^{\dagger}_{\sigma}]_{-} = -\mu_{f\sigma} \hat{f}^{\dagger}_{\sigma} + U_{\mathrm{f}} \hat{f}^{\dagger}_{\sigma} \hat{f}^{\dagger}_{\bar{\sigma}} \hat{f}_{\bar{\sigma}} + U_{\mathrm{fb}} \hat{f}^{\dagger}_{\sigma} \hat{b}^{\dagger} \hat{b} - \sigma g \hat{f}_{\bar{\sigma}} \hat{b}^{\dagger} + \sum_{k} V_{k\sigma} \hat{c}^{\dagger}_{k\sigma}, \tag{A.4}$$

$$[\hat{\mathcal{H}}^{\mathrm{And}}, \hat{c}_{k\sigma}]_{-} = -\varepsilon_{k\sigma} \hat{c}_{k\sigma} - V_{k\sigma} \hat{f}_{\sigma} - \sigma W_k \hat{c}^{\dagger}_{k\bar{\sigma}}, \tag{A.5}$$

$$[\hat{\mathcal{H}}^{\mathrm{And}}, \hat{c}^{\dagger}_{k\sigma}]_{-} = \varepsilon_{k\sigma} \hat{c}^{\dagger}_{k\sigma} + V_{k\sigma} \hat{f}^{\dagger}_{\sigma} + \sigma W_k \hat{c}_{k\bar{\sigma}}, \tag{A.6}$$

where $\bar{\sigma} = -\sigma$.

Now we use the equation of motion (A.1) for the case when $\hat{A} = \hat{f}_{\sigma}$ and $\hat{B} = \hat{f}^{\dagger}_{\sigma}$. In combination with the commutation relation (A.3), we obtain

$$(\mathrm{i}\omega_n + \mu_{f\sigma}) \langle\langle \hat{f}_{\sigma}, \hat{f}^{\dagger}_{\sigma} \rangle\rangle_{\omega} - U_{\mathrm{f}} \langle\langle \hat{f}_{\sigma} \hat{f}^{\dagger}_{\bar{\sigma}} \hat{f}_{\bar{\sigma}}, \hat{f}^{\dagger}_{\sigma} \rangle\rangle_{\omega} - U_{\mathrm{fb}} \langle\langle \hat{f}_{\sigma} \hat{b}^{\dagger} \hat{b}, \hat{f}^{\dagger}_{\sigma} \rangle\rangle_{\omega} + \sigma g \langle\langle \hat{f}^{\dagger}_{\bar{\sigma}} \hat{b}, \hat{f}^{\dagger}_{\sigma} \rangle\rangle_{\omega} - \sum_{k} V_{k\sigma} \langle\langle \hat{c}_{k\sigma}, \hat{f}^{\dagger}_{\sigma} \rangle\rangle_{\omega} = 1. \tag{A.7}$$

To calculate $\langle\langle \hat{c}_{k\sigma}, \hat{f}^{\dagger}_{\sigma} \rangle\rangle_{\omega}$, we again use the equation of motion (A.1), but in this case with $\hat{A} = \hat{c}_{k\sigma}$ and $\hat{B} = \hat{f}^{\dagger}_{\sigma}$. With equation (A.5), we obtain the following relation:

$$(\mathrm{i}\omega_n - \varepsilon_{k\sigma}) \langle\langle \hat{c}_{k\sigma}, \hat{f}^{\dagger}_{\sigma} \rangle\rangle_{\omega} - V_{k\sigma} \langle\langle \hat{f}_{\sigma}, \hat{f}^{\dagger}_{\sigma} \rangle\rangle_{\omega} - \sigma W_k \langle\langle \hat{c}^{\dagger}_{k\bar{\sigma}}, \hat{f}^{\dagger}_{\sigma} \rangle\rangle_{\omega} = 0. \tag{A.8}$$

Finally, to calculate $\langle\langle \hat{c}^{\dagger}_{k\bar{\sigma}}, \hat{f}^{\dagger}_{\sigma} \rangle\rangle_{\omega}$, we use equation (A.1) with $\hat{A} = \hat{c}^{\dagger}_{k\bar{\sigma}}$ and $\hat{B} = \hat{f}^{\dagger}_{\sigma}$, which results in

$$(\mathrm{i}\omega_n + \varepsilon_{k\bar{\sigma}}) \langle\langle \hat{c}^{\dagger}_{k\bar{\sigma}}, \hat{f}^{\dagger}_{\sigma} \rangle\rangle_{\omega} + V_{k\bar{\sigma}} \langle\langle \hat{f}^{\dagger}_{\bar{\sigma}}, \hat{f}^{\dagger}_{\sigma} \rangle\rangle_{\omega} - \sigma W_k \langle\langle \hat{c}_{k\sigma}, \hat{f}^{\dagger}_{\sigma} \rangle\rangle_{\omega} = 0. \tag{A.9}$$

From equations (A.8) and (A.9), we derive

$$\langle\langle \hat{c}_{k\sigma}, \hat{f}^{\dagger}_{\sigma} \rangle\rangle_{\omega} = \frac{V_{k\sigma} (\mathrm{i}\omega_n + \varepsilon_{k\bar{\sigma}})}{(\mathrm{i}\omega_n - \varepsilon_{k\sigma})(\mathrm{i}\omega_n + \varepsilon_{k\bar{\sigma}}) - W_k^2} \langle\langle \hat{f}_{\sigma}, \hat{f}^{\dagger}_{\sigma} \rangle\rangle_{\omega} - \frac{\sigma V_{k\bar{\sigma}} W_k}{(\mathrm{i}\omega_n - \varepsilon_{k\sigma})(\mathrm{i}\omega_n + \varepsilon_{k\bar{\sigma}}) - W_k^2} \langle\langle \hat{f}^{\dagger}_{\bar{\sigma}}, \hat{f}^{\dagger}_{\sigma} \rangle\rangle_{\omega}. \tag{A.10}$$

Now we combine equation (A.10) with (A.7) and obtain

$$(\mathrm{i}\omega_n + \mu_{f\sigma} - \Delta_\sigma(\mathrm{i}\omega_n))G_\sigma(\mathrm{i}\omega_n) - \Delta_{\mathrm{SC}}(\sigma\mathrm{i}\omega_n)F^*(-\sigma\mathrm{i}\omega_n) - U_{\mathrm{f}}Q_{\mathrm{ff}\sigma}(\mathrm{i}\omega_n)$$
$$-U_{\mathrm{fb}}Q_{\mathrm{fb}\sigma}(\mathrm{i}\omega_n) - \sigma g Q^*_{g\bar{\sigma}\sigma}(\mathrm{i}\omega_n) = 1. \tag{A.11}$$

Note that $\langle\langle \hat{f}_\sigma, \hat{f}^\dagger_\sigma\rangle\rangle_\omega \equiv G_\sigma(\mathrm{i}\omega_n)$ is the normal Green's function and $\langle\langle \hat{f}_\uparrow, \hat{f}_\downarrow\rangle\rangle_\omega \equiv F(\omega)$ the superfluid Green's function. We also define

$$\Delta_\sigma(\mathrm{i}\omega_n) = \Delta^*_\sigma(-\mathrm{i}\omega_n)$$
$$= -\sum_k V^2_{k\sigma}\frac{\mathrm{i}\omega_n + \varepsilon_{k\bar{\sigma}}}{(\varepsilon_{k\sigma} - \mathrm{i}\omega_n)(\varepsilon_{k\bar{\sigma}} + \mathrm{i}\omega_n) + W^2_k}, \tag{A.12}$$

$$\Delta_{\mathrm{SC}}(\mathrm{i}\omega_n) = \Delta^*_{\mathrm{SC}}(-\mathrm{i}\omega_n)$$
$$= \sum_k \frac{V_{k\uparrow}V_{k\downarrow}W_k}{(\varepsilon_{k\uparrow} - \mathrm{i}\omega_n)(\varepsilon_{k\downarrow} + \mathrm{i}\omega_n) + W^2_k}, \tag{A.13}$$

which are the normal and the superfluid hybridization functions, respectively, and the following correlation functions: $Q_{\mathrm{ff}\sigma}(\mathrm{i}\omega_n) = \langle\langle \hat{f}_\sigma \hat{f}^\dagger_{\bar{\sigma}}\hat{f}_{\bar{\sigma}}, \hat{f}^\dagger_\sigma\rangle\rangle_\omega$, $Q_{\mathrm{ff}\sigma\bar{\sigma}}(\mathrm{i}\omega_n) = \langle\langle \hat{f}_\sigma \hat{f}^\dagger_{\bar{\sigma}}\hat{f}_{\bar{\sigma}}, \hat{f}_{\bar{\sigma}}\rangle\rangle_\omega$, $Q_{\mathrm{fb}\sigma}(\mathrm{i}\omega_n) = \langle\langle \hat{f}_\sigma \hat{b}^\dagger\hat{b}, \hat{f}^\dagger_\sigma\rangle\rangle_\omega$, $Q_{\mathrm{fb}\sigma\bar{\sigma}}(\mathrm{i}\omega_n) = \langle\langle \hat{f}_\sigma \hat{b}^\dagger\hat{b}, \hat{f}_{\bar{\sigma}}\rangle\rangle_\omega$, $Q_{g\sigma}(\mathrm{i}\omega_n) = \langle\langle \hat{f}_\sigma \hat{b}^\dagger, \hat{f}^\dagger_\sigma\rangle\rangle_\omega$ and $Q_{g\sigma\bar{\sigma}}(\mathrm{i}\omega_n) = \langle\langle \hat{f}_\sigma \hat{b}^\dagger, \hat{f}_{\bar{\sigma}}\rangle\rangle_\omega$.

To obtain the self-energy we need to derive one more equation. For this purpose, we again use the equation of motion (A.1) and take $\hat{A} = \hat{f}^\dagger_\sigma$ and $\hat{B} = \hat{f}^\dagger_{\bar{\sigma}}$. Based on equation (A.4), we obtain

$$(\mathrm{i}\omega_n - \mu_{f\sigma})\langle\langle \hat{f}^\dagger_\sigma, \hat{f}^\dagger_{\bar{\sigma}}\rangle\rangle_\omega + U_{\mathrm{f}}\langle\langle \hat{f}^\dagger_\sigma \hat{f}^\dagger_{\bar{\sigma}}\hat{f}_{\bar{\sigma}}, \hat{f}^\dagger_{\bar{\sigma}}\rangle\rangle_\omega + U_{\mathrm{fb}}\langle\langle \hat{f}^\dagger_\sigma \hat{b}^\dagger\hat{b}, \hat{f}^\dagger_{\bar{\sigma}}\rangle\rangle_\omega - \sigma g\langle\langle \hat{f}_{\bar{\sigma}}\hat{b}^\dagger, \hat{f}^\dagger_{\bar{\sigma}}\rangle\rangle_\omega$$
$$+\sum_k V_{k\sigma}\langle\langle \hat{c}^\dagger_{k\sigma}, \hat{f}^\dagger_{\bar{\sigma}}\rangle\rangle_\omega = 0. \tag{A.14}$$

We now replace $\langle\langle \hat{c}^\dagger_{k\sigma}, \hat{f}^\dagger_{\bar{\sigma}}\rangle\rangle_\omega$ using equation (A.10) and obtain:

$$-\sigma(\mathrm{i}\omega_n - \mu_{f\sigma} + \Delta^*_\sigma(\mathrm{i}\omega_n))F^*(\sigma\mathrm{i}\omega_n) + \sigma\Delta_{\mathrm{SC}}(-\sigma\mathrm{i}\omega_n)G_{\bar{\sigma}}(\mathrm{i}\omega_n) - U_{\mathrm{f}}Q^*_{\mathrm{ff},\sigma\bar{\sigma}}(\mathrm{i}\omega_n)$$
$$-U_{\mathrm{fb}}Q^*_{\mathrm{fb}\sigma\bar{\sigma}}(\mathrm{i}\omega_n) - \sigma g Q_{g\bar{\sigma}}(\mathrm{i}\omega_n) = 0. \tag{A.15}$$

We proceed to write our results in matrix form. For $\sigma = 1$, we use equation (A.11) and the complex conjugate of equation (A.15), whereas for $\sigma = -1$, we take equation (A.15) and the complex conjugate of equation (A.11):

$$(\mathrm{i}\omega_n + \mu_{f\uparrow} - \Delta_\uparrow(\mathrm{i}\omega_n))G_\uparrow(\mathrm{i}\omega_n) - \Delta_{\mathrm{SC}}(\mathrm{i}\omega_n)F^*(-\mathrm{i}\omega_n) - U_{\mathrm{f}}Q_{\mathrm{ff}\uparrow}(\mathrm{i}\omega_n)$$
$$-U_{\mathrm{fb}}Q_{\mathrm{fb}\uparrow}(\mathrm{i}\omega_n) - g Q^*_{g\downarrow\uparrow}(\mathrm{i}\omega_n) = 1,$$
$$-\left(\mathrm{i}\omega_n - \mu_{f\downarrow} + \Delta_\downarrow(-\mathrm{i}\omega_n)\right)G^*_\downarrow(\mathrm{i}\omega_n) - \Delta_{\mathrm{SC}}(\mathrm{i}\omega_n)F(\mathrm{i}\omega_n) - U_{\mathrm{f}}Q^*_{\mathrm{ff}\downarrow}(\mathrm{i}\omega_n)$$
$$-U_{\mathrm{fb}}Q^*_{\mathrm{fb}\downarrow}(\mathrm{i}\omega_n) + g Q_{g\uparrow\downarrow}(\mathrm{i}\omega_n) = 1,$$
$$\left(\mathrm{i}\omega_n + \mu_{f\uparrow} - \Delta_\uparrow(\mathrm{i}\omega_n)\right)F(\mathrm{i}\omega_n) + \Delta_{\mathrm{SC}}(\mathrm{i}\omega_n)G^*_\downarrow(\mathrm{i}\omega_n) - U_{\mathrm{f}}Q_{\mathrm{ff},\uparrow\downarrow}(\mathrm{i}\omega_n)$$
$$-U_{\mathrm{fb}}Q_{\mathrm{fb}\uparrow\downarrow}(\mathrm{i}\omega_n) - g Q^*_{g\downarrow}(\mathrm{i}\omega_n) = 0,$$

$$(\mathrm{i}\omega_n - \mu_{f\downarrow} + \Delta_\downarrow(\mathrm{i}\omega_n))F^*(\mathrm{i}\omega_n) - \Delta_{\mathrm{SC}}(\mathrm{i}\omega_n)G_\uparrow(\mathrm{i}\omega_n) - U_\mathrm{f}Q^*_{\mathrm{ff},\downarrow\uparrow}(\mathrm{i}\omega_n)$$
$$-U_\mathrm{fb}Q^*_{\mathrm{fb}\downarrow\uparrow}(\mathrm{i}\omega_n) + gQ_{g\uparrow}(\mathrm{i}\omega_n) = 0.$$

The last four equations can be rewritten in matrix form as follows:

$$\begin{pmatrix}1 & 0\\ 0 & 1\end{pmatrix} = \begin{pmatrix}\mathrm{i}\omega_n + \mu_{\mathrm{f}\uparrow} - \Delta_\uparrow(\mathrm{i}\omega_n) & -\Delta_{\mathrm{SC}}(\mathrm{i}\omega_n)\\ -\Delta_{\mathrm{SC}}(\mathrm{i}\omega_n) & \mathrm{i}\omega_n - \mu_{\mathrm{f}\downarrow} + \Delta_\downarrow(-\mathrm{i}\omega_n)\end{pmatrix}\begin{pmatrix}G_\uparrow(\mathrm{i}\omega_n) & F(\mathrm{i}\omega_n)\\ F^*(-\mathrm{i}\omega_n) & -G^*_\downarrow(\mathrm{i}\omega_n)\end{pmatrix}$$
$$-\begin{pmatrix}U_\mathrm{f}Q_{\mathrm{ff}\uparrow}(\mathrm{i}\omega_n) + U_\mathrm{fb}Q_{\mathrm{fb}\uparrow}(\mathrm{i}\omega_n) + gQ^*_{g\downarrow\uparrow}(\mathrm{i}\omega_n) & U_\mathrm{f}Q_{\mathrm{ff},\uparrow\downarrow}(\mathrm{i}\omega_n) + U_\mathrm{fb}Q_{\mathrm{fb}\uparrow\downarrow}(\mathrm{i}\omega_n) + gQ^*_{g\downarrow}(\mathrm{i}\omega_n)\\ U_\mathrm{f}Q^*_{\mathrm{ff},\downarrow\uparrow}(\mathrm{i}\omega_n) + U_\mathrm{fb}Q^*_{\mathrm{fb}\downarrow\uparrow}(\mathrm{i}\omega_n) - gQ_{g\uparrow}(\mathrm{i}\omega_n) & U_\mathrm{f}Q^*_{\mathrm{ff}\downarrow}(\mathrm{i}\omega_n) + U_\mathrm{fb}Q^*_{\mathrm{fb}\downarrow}(\mathrm{i}\omega_n) - gQ_{g\uparrow\downarrow}(\mathrm{i}\omega_n)\end{pmatrix}. \tag{A.16}$$

Now we compare equation (A.16) with the Dyson equation, which has the matrix form:

$$\hat{\mathcal{G}}^{-1}(\mathrm{i}\omega_n) - \hat{\Sigma}(\mathrm{i}\omega_n) = \hat{G}^{-1}(\mathrm{i}\omega_n)\,, \tag{A.17}$$

where

$$\hat{G}(\mathrm{i}\omega) = \begin{pmatrix}G_\uparrow(\mathrm{i}\omega_n) & F(\mathrm{i}\omega_n)\\ F^*(-\mathrm{i}\omega_n) & -G^*_\downarrow(\mathrm{i}\omega_n)\end{pmatrix} \tag{A.18}$$

is the matrix interacting Green's function,

$$\hat{\mathcal{G}}(\mathrm{i}\omega) = \begin{pmatrix}\mathrm{i}\omega_n + \mu_{\mathrm{f}\uparrow} - \Delta_\uparrow(\mathrm{i}\omega_n) & -\Delta_{\mathrm{SC}}(\mathrm{i}\omega_n)\\ -\Delta_{\mathrm{SC}}(\mathrm{i}\omega_n) & \mathrm{i}\omega_n - \mu_{\mathrm{f}\downarrow} + \Delta_\downarrow(-\mathrm{i}\omega_n)\end{pmatrix}^{-1} \tag{A.19}$$

is the matrix Weiss Green's function and $\hat{\Sigma}(\omega)$ is the matrix self-energy. From this comparison it follows directly that

$$\begin{pmatrix}\Sigma_\uparrow(\mathrm{i}\omega_n) & \Sigma_{\mathrm{SC}}(\mathrm{i}\omega_n)\\ \Sigma^*_{\mathrm{SC}}(\mathrm{i}\omega_n) & -\Sigma^*_\downarrow(\mathrm{i}\omega_n)\end{pmatrix}$$
$$= \begin{pmatrix}U_\mathrm{f}Q_{\mathrm{ff}\uparrow}(\mathrm{i}\omega_n) + U_\mathrm{fb}Q_{\mathrm{fb}\uparrow}(\mathrm{i}\omega_n) + gQ^*_{g\downarrow\uparrow}(\mathrm{i}\omega_n) & U_\mathrm{f}Q_{\mathrm{ff},\uparrow\downarrow}(\mathrm{i}\omega_n) + U_\mathrm{fb}Q_{\mathrm{fb}\uparrow\downarrow}(\mathrm{i}\omega_n) + gQ^*_{g\downarrow}(\mathrm{i}\omega_n)\\ U_\mathrm{f}Q^*_{\mathrm{ff},\downarrow\uparrow}(\mathrm{i}\omega_n) + U_\mathrm{fb}Q^*_{\mathrm{fb}\downarrow\uparrow}(\mathrm{i}\omega_n) - gQ_{g\uparrow}(\mathrm{i}\omega_n) & U_\mathrm{f}Q^*_{\mathrm{ff}\downarrow}(\mathrm{i}\omega_n) + U_\mathrm{fb}Q^*_{\mathrm{fb}\downarrow}(\mathrm{i}\omega_n) - gQ_{g\uparrow\downarrow}(\mathrm{i}\omega_n)\end{pmatrix}$$
$$\times\begin{pmatrix}G_\uparrow(\mathrm{i}\omega_n) & F(\mathrm{i}\omega_n)\\ F^*(-\mathrm{i}\omega_n) & -G^*_\downarrow(\mathrm{i}\omega_n)\end{pmatrix}^{-1}. \tag{A.20}$$

From here we obtain the final result:

$$\Sigma_\sigma(\mathrm{i}\omega_n) = \frac{(U_\mathrm{f}Q_{\mathrm{ff}\sigma}(\mathrm{i}\omega_n) + U_\mathrm{fb}Q_{\mathrm{fb}\sigma}(\mathrm{i}\omega_n) + \sigma g Q^*_{g\bar{\sigma}\sigma}(\mathrm{i}\omega_n))G^*_{\bar{\sigma}}(\mathrm{i}\omega_n)}{G_\sigma(\mathrm{i}\omega_n)G^*_{\bar{\sigma}}(\mathrm{i}\omega_n) + F(\sigma\mathrm{i}\omega_n)F^*(\bar{\sigma}\mathrm{i}\omega_n)}$$
$$+\frac{(\sigma U_\mathrm{f}Q_{\mathrm{ff},\sigma\bar{\sigma}}(\mathrm{i}\omega_n) + \sigma U_\mathrm{fb}Q_{\mathrm{fb}\sigma\bar{\sigma}}(\mathrm{i}\omega_n) + gQ^*_{g\bar{\sigma}}(\mathrm{i}\omega_n))F^*(\bar{\sigma}\mathrm{i}\omega_n)}{G_\sigma(\mathrm{i}\omega_n)G^*_{\bar{\sigma}}(\mathrm{i}\omega_n) + F(\sigma\mathrm{i}\omega_n)F^*(\bar{\sigma}\mathrm{i}\omega_n)}, \tag{A.21}$$

$$\Sigma_{\mathrm{SC}}(\mathrm{i}\omega_n) = \frac{(U_\mathrm{f}Q_{\mathrm{ff}\uparrow}(\mathrm{i}\omega_n) + U_\mathrm{fb}Q_{\mathrm{fb}\uparrow}(\mathrm{i}\omega_n) + gQ^*_{g\downarrow\uparrow}(\mathrm{i}\omega_n))F(\mathrm{i}\omega_n)}{G_\uparrow(\mathrm{i}\omega_n)G^*_\downarrow(\mathrm{i}\omega_n) + F(\mathrm{i}\omega_n)F^*(-\mathrm{i}\omega_n)}$$
$$-\frac{(U_\mathrm{f}Q_{\mathrm{ff},\uparrow\downarrow}(\mathrm{i}\omega_n) + U_\mathrm{fb}Q_{\mathrm{fb}\uparrow\downarrow}(\mathrm{i}\omega_n) + gQ^*_{g\downarrow}(\mathrm{i}\omega_n))G_\uparrow(\mathrm{i}\omega_n)}{G_\uparrow(\mathrm{i}\omega_n)G^*_\downarrow(\mathrm{i}\omega_n) + F(\mathrm{i}\omega_n)F^*(-\mathrm{i}\omega_n)}. \tag{A.22}$$

References

[1] Anderson M H, Ensher J R, Matthews M R, Wieman C E and Cornell E A 1995 *Science* **269** 198
[2] Bradley C C, Sackett C A, Tollett J J and Hulet R G 1995 *Phys. Rev. Lett.* **75** 1687
[3] Davis K B, Mewes M O, Andrews M R, van Druten N J, Durfee D S, Kurn D M and Ketterle W 1995 *Phys. Rev. Lett.* **75** 3969
[4] De Marco and Jin D C 1999 *Science* **285** 1703
[5] Schreck F, Khaykovich L, Corwin K L, Ferrari G, Bourdel T, Cubizollles J and Salomon C 2001 *Phys. Rev. Lett.* **87** 080403
[6] Truscott A G, Strecker K E, Mc Alexander W I, Partidge G B and Hulet R G 2001 *Science* **291** 2570
[7] Greiner M, Regal C A and Jin D S 2003 *Nature* **426** 537
[8] Jochim S, Bartenstein M, Altmeyer A, Hendl G, Riedl S, Chin C, Hecker Denschlag J and Grimm R 2003 *Science* **302** 2101
[9] Zwierlein M W, Stan C A, Schunck C H, Raupach S M F, Gupta S, Hadzibabic Z and Ketterle W 2003 *Phys. Rev. Lett.* **91** 250401
[10] Bourdel T, Khaykovich L, Cubizolles J, Zhang J, Chevy F, Teichmann M, Tarruell L, Kokkelmans S J J M F and Salomon C 2004 *Phys. Rev. Lett.* **93** 050401
[11] Zwierlein M W, Abo-Shaeer J R, Schirotzek A, Schunck C H and Ketterle W 2005 *Nature* **435** 1047
[12] Zwierlein M W, Schirotzek A, Schunck C H and Ketterle W 2006 *Science* **311** 492
[13] Zwierlein M W, Schunck C H, Schirotzek A and Ketterle W 2006 *Science* **442** 54
[14] Partridge G B, Li W, Kamar R I, Liao Y A and Hulet R G 2006 *Science* **311** 503
[15] Shin Y, Schunck C H, Schirotzek A and Ketterle W 2008 *Nature* **451** 689
[16] Taglieber T, Voigt A C, Aoki T, Hänsch T W and Dieckmann K 2008 *Phys . Rev. Lett.* **100** 010401
[17] Wille E *et al* 2008 *Phys. Rev. Lett.* **100** 053201
[18] Modugno G, Ferlaino F, Heidemann R, Roati G and Inguscio M 2003 *Phys. Rev.* A **68** 011601
[19] Stöferle T, Moritz H, Günter K, Köhl M and Esslinger T 2006 *Phys. Rev. Lett.* **96** 030401
[20] Chin J K, Miller D E, Liu Y, Stan C, Setiawan W, Sanner C, Xu K and Ketterle W 2006 *Nature* **443** 961
[21] Rom T, Best Th, van Oosten D, Schneider U, Fölling S, Paredes B and Bloch I 2006 *Nature* **444** 733
[22] Jördens R, Strohmaier N, Günter K, Moritz H and Esslinger T 2008 *Nature* **455** 204
[23] Schneider U, Hackermüller L, Will S, Best Th, Bloch I, Costi T A, Helmes R W, Rasch D and Rosch A 2008 *Science* **322** 1520
[24] Zhou F and Wu C 2006 *New J. Phys.* **8** 166
[25] Watanabe R and Imada M 2009 *Phys. Rev.* A **80** 043624
[26] Zhai H and Ho T-L 2007 *Phys. Rev. Lett.* **99** 100402
[27] Titvinidze I, Snoek M and Hofstetter W 2008 *Phys. Rev. Lett.* **100** 100401
[28] Titvinidze I, Snoek M and Hofstetter W 2009 *Phys. Rev.* B **79** 144506
[29] Metzner W and Vollhardt D 1989 *Phys. Rev. Lett.* **62** 324
[30] Georges A, Kotliar G, Krauth W and Rozenberg M J 1996 *Rev. Mod. Phys.* **68** 13
[31] Rokhsar D S and Kotliar B G 1991 *Phys. Rev.* B **44** 10328
[32] Sheshadri K, Krishnamurthy H R, Pandit R and Ramakrishnan T V 1993 *Europhys. Lett.* **22** 257
[33] Fisher M P A, Weichman P B, Grinstein G and Fisher D S 1989 *Phys. Rev.* B **40** 546
[34] Duan L-M 2006 *Phys. Rev. Lett.* **96** 103201
[35] Koetsier A, Dickerscheid D B M and Stoof H T C 2006 *Phys. Rev.* A **74** 033621
[36] Dickerscheid D B M, Khawaja Al U, Oosten D and van Stoof H T C 2005 *Phys. Rev.* A **71** 043604
[37] Dickerscheid D B M and Stoof H T C 2005 *Phys. Rev.* A **72** 053625
[38] Diener R B and Ho T-L 2005 *Phys. Rev. Lett.* **96** 010402
[39] Gubbels K B, Dickerscheid D B M and Stoof H T C 2006 *New J. Phys.* **8** 151
[40] Holland M, Kokkelmans S J J M F, Chiofalo M L and Walser R 2001 *Phys. Rev. Lett.* **87** 120406
[41] Carr L D and Holland M J 2005 *Phys. Rev.* A **72** 031604

[42] Busch T, Englert B-G, Rzążewski K and Wilkens M 1998 *Found. Phys.* **28** 549
[43] Petrov D S, Salomon C and Shlyapnikov G V 2004 *Phys. Rev. Lett.* **93** 090404
[44] Petrov D S, Salomon C and Shlyapnikov G V 2005 *Phys. Rev.* A **71** 012708
[45] Abramowitz M and Stegun I A 1964 *Handbook of Mathematicsal Functions* (New York: Dover)
[46] Georges A, Kotliar G, Krauth W and Rozenberg M J 1996 *Rev. Mod. Phys.* **68** 13
[47] Caffarel M and Krauth W 1994 *Phys. Rev. Lett.* **72** 1545
[48] Si Q, Rozenberg M J, Kotliar K and Ruckenstein A E 1994 *Phys. Rev. Lett.* **72** 2761
[49] Toschi A, Capone M and Castellani C 2005 *Phys. Rev.* B **72** 235118
[50] Regal C A, Greiner M and Jin D S 2005 *Phys. Rev. Lett.* **92** 040403
[51] Keller M, Metzner W and Schollwöck O 2001 *Phys. Rev. Lett.* **86** 4612
[52] Toschi A, Barone P, Capone M and Castellani C 2005 *New J. Phys.* **7** 7